A Journal of the Gesellschaft Deutscher Chemiker

Angewandte International Edition

GDCh

Chemie

www.angewandte.org

Accepted Article

Title: Fe Single Atom on MoS2 Nanosheets for N2 Electroreduction into Ammonia

Authors: Hongyang Su, Lanlan Chen, Yizhen Chen, Yuting Wu, Xiaonan Wu, Rui Si, Wenhua Zhang, Zhigang Geng, and Jie Zeng

To be cited as: *Angew. Chem. Int. Ed.* 10.1002/anie.202009217

Link to VoR: https://doi.org/10.1002/anie.202009217

WILEY-VCH

10.1002/anie.202009217

Fe Single Atom on MoS_2 Nanosheets for N_2 Electroreduction into Ammonia

Hongyang Su, Lanlan Chen, Yizhen Chen, Rui Si, Yuting Wu, Xiaonan Wu, Zhigang Geng, Wenhua Zhang,* and Jie Zeng**

H. Su,[†] Y. Chen,[†] Y. Wu, X. Wu, Dr. Z. Geng, Prof. J. Zeng
Hefei National Laboratory for Physical Sciences at the Microscale, CAS Key Laboratory of Strongly-Coupled Quantum Matter Physics, Key Laboratory of Surface and Interface Chemistry and Energy Catalysis of Anhui Higher Education Institutes, Department of Chemical Physics, University of Science and Technology of China, Hefei, Anhui 230026, P. R. China.
E-mail: gengzg@ustc.edu.cn (Z.G.), zengj@ustc.edu.cn (J. Z.)

L. Chen,[†] Prof. W. Zhang
Hefei National Laboratory for Physical Sciences at the Microscale, CAS Key Laboratory of Materials for Energy Conversion and Synergetic Innovation Centre of Quantum Information & Quantum Physics, University of Science and Technology of China, Hefei, Anhui 230026, P. R. China.
E-mail: whhzhang@ustc.edu.cn (W. Z.)

Prof. R. Si
Shanghai Synchrotron Radiation Facility, Shanghai Advanced Research Institute, Chinese Academy of Sciences, Shanghai 201210, P.R. China.

[†]These authors contributed equally to this work.

[**]This work was supported by National Science Fund for Distinguished Young Scholars (21925204), NSFC (U1932146 and U19A2015), National Key Research and Development Program of China (2019YFA0405600, 2018YFA0208600), Key Research Program of Frontier

Sciences of the CAS (QYZDB-SSW-SLH017), Fundamental Research Funds for the Central Universities, and USTC Research Funds of the Double First-Class Initiative (YD2340002002). All the calculations are performed on the supercomputing system in USTC-SCC and Guangzhou-SCC. Y. Chen gratefully acknowledge the China Scholarship Council (CSC. No. 201806340062) for financial support.

10.1002/anie.202009217

Abstract

Ammonia (NH_3) plays a pivotal role in our daily life considering its wide applications in fertilizer industry. Many efforts have been devoted to achieving highly efficient artificial synthesis of ammonia. Herein, we reported a novel Fe-MoS_2 catalyst with Fe atomically dispersed on MoS_2 nanosheets by imitating the natural nitrogenase to boost N_2 electroreduction into NH_3 at room temperature. The Fe-MoS_2 nanosheets exhibited a faradic efficiency of 18.8% with a yield rate of 8.63 μg_{NH_3} $mg_{cat.}^{-1}$ h^{-1} for NH_3 at -0.3 V versus reversible hydrogen electrode. The mechanism study revealed that the electroreduction of N_2 was promoted and the competing hydrogen evolution reaction was suppressed by decorating the edge sites of S in the MoS_2 with the atomically dispersed Fe, resulting in the high catalytic performance for the electroreduction of N_2 into NH_3. This work would provide new ideas for the design of catalysts for N_2 electroreduction and strengthen our understanding about the N_2 activation on Mo-based catalysts.

Keywords: Fe-MoS_2 catalysts, N_2 activation, N_2 electroreduction, NH_3 production, HER suppression

Table of Contents

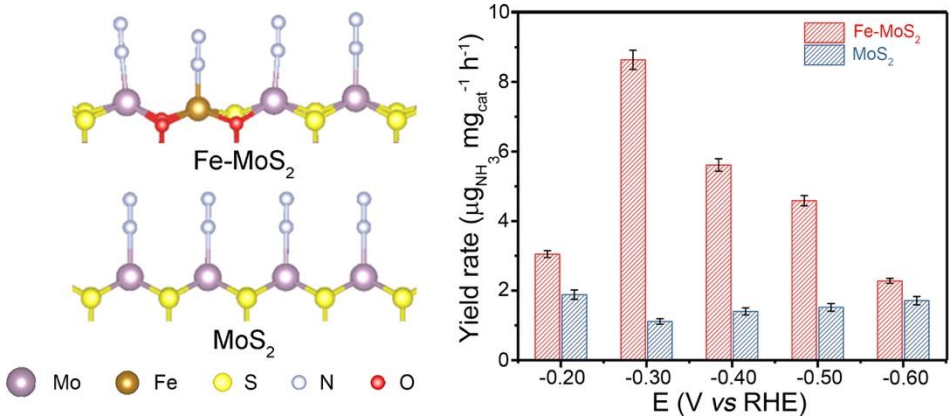

Introduction

Ammonia (NH_3) serves as an important precursor of fertilizers and industrial chemical stock for daily life, thus the artificial synthesis of ammonia has attracted lots of attention in the past century.[1-5] The Haber-Bosch process has been the most common industrial reaction for the production of NH_3. Due to the inert N_2 molecule (with a dissociation energy of 945 kJ mol^{-1} for the strong triple bond),[6] the industrialized Haber-Bosch process needs to be operated at high temperature and pressure, which costs approximately 1-2% of the total global energy consumption so far.[7-10] Considering the harsh condition of Haber-Bosch process and the consequent emission of greenhouse gas, there is an urgent need to develop an alternative method to achieve highly efficient synthesis of NH_3 at milder conditions.

The electroreduction of N_2 into NH_3 serve as a safe, low-cost, and environmentally friendly approach by using renewable energy source at the ambient temperature and pressure in the past decade.[11-16] Among the catalysts for N_2 electroreduction, Mo-based catalysts were believed as promising candidates for N_2 activation from the prediction by theoretical calculations.[17-20] Besides, many efforts have been devoted to achieving the electroreduction of N_2 into NH_3 with Mo-based catalysts including Mo single atoms, sulfides, nitrides, and carbides.[21-25] Among these Mo-containing compounds, MoS_2 is deemed as a desirable catalyst for N_2 electroreduction owing to the similar Mo-S structures as those in the presence of natural nitrogenase.[26] However, MoS_2 usually exhibits considerable activity for hydrogen evolution reaction (HER), which serves as a primary competing reaction of N_2 electroreduction at similar applied potentials.[27] In addition, the edge sites of S atoms in MoS_2 are reported to play an important role in HER as they are usually considered as the active sites for the reduction of proton.[28,29] Therefore, the exploration of a MoS_2-based electrocatalyst by suppressing the activity of HER is necessary to achieve transformative advances towards N_2 electroreduction.

Herein, we reported a novel Fe-MoS_2 catalyst with the atomically dispersed Fe on MoS_2 nanosheets with excellent performance towards N_2 electroreduction by greatly suppressing HER activity. In the H-cell system with 0.5 M K_2SO_4 (pH = 3) as electrolyte, the obtained Fe-MoS_2 catalysts exhibited a yield rate of NH_3 with 8.63 μg_{NH_3} $mg_{cat.}^{-1}$ h^{-1} at -0.3 V versus reversible hydrogen electrode potential (*vs* RHE), 7.77 times of that (1.11 μg_{NH_3} $mg_{cat.}^{-1}$ h^{-1}) for MoS_2. Specially, at -0.3 V *vs* RHE, the Faradic efficiency of NH_3 (FE_{NH_3}) for Fe-MoS_2 nanosheets

reached 18.8%, whereas the FE_{NH_3} for MoS_2 nanosheets was only 2.23%. The mechanism study revealed that the N_2 electroreduction was facilitated on Fe-MoS_2 as the energy barrier of the potential-determining step (PDS) for Fe-MoS_2 was 0.37 eV, lower than that (0.50 eV) for MoS_2. Moreover, the energy barrier for HER over Fe-MoS_2 was 0.15 eV, which was higher than that (0.03 eV) of MoS_2. As such, the introduction of atomically dispersed Fe on MoS_2 nanosheets suppressed the competing HER, thus enhancing the catalytic performance towards N_2 electroreduction.

Fe-MoS_2 catalysts were prepared by injecting $FeCl_3$ solution into a mixture containing water, ethanol and MoS_2 nanosheets with the use of a syringe pump (see details in Supporting information). Figure 1a shows scanning electron microscopy (SEM) image of the Fe-MoS_2. The morphology of the obtained Fe-MoS_2 was similar as MoS_2 nanosheets (Fig. S1). Figure 1b shows the high-angle annular dark field scanning transmission electron microscopy (HAADF-STEM) image of Fe-MoS_2 nanosheets. the lattice fringe with an interplanar spacing of 0.27 nm was ascribed to the (100) plane of hexagonal MoS_2.[30] The high-resolution transmission electron microscopy (HRTEM) image in Figure S2 shows that the layer spacing for Fe-MoS_2 nanosheets was approximately 0.66 nm, ascribed to the (002) crystalline plane for MoS_2.[31] The result revealed that the crystalline structure of MoS_2 was not changed. The energy dispersive X-ray (EDX) elemental mapping images clearly showed that the element of Fe, Mo, and S dispersed homogeneously through the whole Fe-MoS_2 nanosheets (Fig. 1c). The concentration of Fe was quantitively determined as 5.3 at% by the inductively coupled plasma atomic emission spectroscopy (ICP-AES). Powder X-ray diffraction (PXRD) and Raman spectroscopy further confirmed that there were no new phases formed since Fe-MoS_2 nanosheets exhibited similar feature peaks as MoS_2 (Fig. S3).

To explore the electronic structure and coordination environment of the Fe-MoS_2 nanosheets, we conducted more characterizations by employing X-ray photoelectron spectroscopy (XPS), ^{57}Fe Mössbauer spectroscopy, and X-ray absorption fine structure spectroscopy (XAFS). In Mo 3*d* spectra, the two peaks located at 229.6 and 232.8 eV represented the Mo $3d_{5/2}$ and Mo $3d_{3/2}$ peaks of MoS_2 (Fig. S4). In the S 2*p* spectrum of Fe-MoS_2 nanosheets, two peaks located at 162.4 and 163.6 eV peak at were assigned to the S $2p_{3/2}$ and S $2p_{1/2}$ peaks for the bonding of Mo-S. In addition, we also observed a new group of feature peaks located at the binding energy of 161.4 eV for S $2p_{3/2}$ and 162.6 eV for S $2p_{1/2}$, which should be

assigned to S bonded with Fe atoms (Fig. 1d).[32,33] Fe 2*p* spectra were also used to uncover more information of Fe species in Fe-MoS_2 nanosheets (Fig. 1e). In the Fe $2p_{3/2}$ region, there was a feature peak located at ~707.9 eV, further confirming the formation of Fe-S bond.[34] Besides, the peak at 709.9 eV was ascribed to the contributions of Fe-O bonds.[35] The ^{57}Fe Mössbauer spectra revealed that the coordination number of Fe was four according to the isomer shift (IS) and quadrupole splitting (QS) value of the spectra (Fig. S5 and Table S1).[36] The spectra can be well fitted with two doublets. The quadrupole doublet with an IS of 0.27 mm s^{-1} and a QS of 0.86 mm s^{-1} was attributed to the coordination between Fe and S.[37] The quadrupole doublet with an IS of 0.36 mm s^{-1} and a QS of 0.44 mm s^{-1} was assigned to the Fe-O bond.[38] The X-ray absorption near-edge spectroscopy (XANES) collected at Fe K edge delivered more information about the chemical state of Fe species in Fe-MoS_2 nanosheets (Fig. 1f). For comparison, Fe foil and Fe_2O_3 standard profiles were also provided. The edge position of Fe-MoS_2 nanosheets (7124.7 eV) was located at the energy between Fe foil (7112.0 eV) and Fe_2O_3 (7126.6 eV) in the XANES spectra, which demonstrated the cationic nature of the Fe (Fig. S6).[39] Based on the fitting results of the EXAFS data of Fe-MoS_2 nanosheets (Figs. S7, S8 and Table S2), we concluded that Fe was present as single-atom species supported on MoS_2 nanosheets, with no evidence of Fe-Fe contributions. The Fe-O coordination number was approximately 3 at a distance of 2.00 Å and the Fe-S coordination number was about 1 at a distance of 2.34 Å. We inferred that Fe-O bonds were formed due to the partial oxidation of Fe in the presence of air and water.

To evaluate the catalytic performance of Fe-MoS_2 nanosheets for N_2 electroreduction, we conducted the electrochemical measurements in the electrolyte of 0.5 M K_2SO_4 (pH = 3) with an H-cell (Fig. S9). The linear sweep voltammetry (LSV) measurement was conducted at a sweep rate of 10 mV s^{-1} for both Fe-MoS_2 and MoS_2 nanosheets (Fig. S10). Fe-MoS_2 nanosheets exhibited higher current density (*j*) in N_2-saturated electrolyte than that in Ar-saturated electrolyte. The difference in the *j* was especially obvious in the potential range from -0.2 to -0.6 V *vs* RHE, implying the potential activity of Fe-MoS_2 nanosheets for N_2 electroreduction (in the inset of Fig. S10). Figure 2a shows the partial *j* of NH_3 (j_{NH_3}) for Fe-MoS_2 and MoS_2 nanosheets. At all of applied potentials, Fe-MoS_2 nanosheets exhibited higher j_{NH_3} than MoS_2 nanosheets. Notably, at -0.3 V *vs* RHE, the j_{NH_3} was 30.8 μA cm^{-2} in the presence of Fe-MoS_2 nanosheets, which was nearly four times higher than that (8.1 μA cm^{-2}) of MoS_2 nanosheets. As shown in

Figure 2b, the FE_{NH_3} for Fe-MoS_2 nanosheets were higher than that for MoS_2 nanosheets at all of applied potentials. At -0.3 V *vs* RHE, the FE_{NH_3} for Fe-MoS_2 nanosheets reached 18.8%, whereas the FE_{NH_3} for MoS_2 nanosheets was only 2.23%. Figure 2c showed the yield rate of NH_3 for Fe-MoS_2 and MoS_2 nanosheets at all of applied potentials. Specially, at -0.3 V *vs* RHE, the yield rate of NH_3 for Fe-MoS_2 nanosheets reached 8.63 μg_{NH_3} $mg_{cat.}^{-1}$ h^{-1}, which was 7.77 times higher than that (1.11 μg_{NH_3} $mg_{cat.}^{-1}$ h^{-1}) for MoS_2 nanosheets (Figs. S11-S14). Apart from the product of NH_3, we also detected the by-product of hydrazine following the four-electron process via the Watt-and-Chrisp method (Fig. S15).[40] It is revealed that there was no hydrazine formed in our experiment, demonstrating the high selectivity of NH_3 for Fe-MoS_2 nanosheets. To confirm that NH_3 derived from N_2 electroreduction over Fe-MoS_2 nanosheets, we also conducted a series of controlled experiments under various conditions. As the results shown in Figure S16, no NH_3 was produced after the electrolysis over Fe-MoS_2 nanosheets in N_2-saturated electrolyte at open-circuit voltage (OCP), indicating little interference of NH_3 from N_2 feeding gas. After electrolysis over Fe-MoS_2 nanosheets in Ar-saturated electrolyte at 0.3 V *vs* RHE for 2 h, the yield of NH_3 was undetectable, indicating that the self-electrolysis of catalysts did not produce NH_3 during the electrocatalysis process. To exclude the catalytic activity of carbon paper, we conducted N_2 electroreduction over carbon paper at -0.3 V *vs* RHE and the yield of NH_3 cannot be determined either. Besides, to exclude the influence of Nafion membrane, we used Nafion membrane as cathode to investigate the contamination of Nafion membrane. After the Nafion membrane was electrolyzed in N_2-saturated 0.5 M K_2SO_4 (pH =3) at -0.3 V *vs* RHE for 2 h, NH_3 was below the detecting limitation. In addition, we sonicated 2×2 cm^2 of both Nafion membrane and nitrile glove in 30 mL of our electrolyte for 2 h, respectively. The results indicated that neither Nafion membrane nor nitrile glove caused any NH_3 contamination. Furthermore, we conducted an isotopic labeling experiment over Fe-MoS_2 nanosheets with $^{15}N_2$ as the feed gas to further verify the origination of NH_3. The concentration of $^{15}NH_4^+$ was determined as 0.124 μg mL^{-1} via the ^1H nuclear magnetic resonance (^{1}HNMR), which was almost equal to that of NH_4^+ (0.122 μg mL^{-1}) in our N_2 experiments, confirming that NH_3 mainly derived from N_2 electroreduction (Figs. S14 and S17). In the long-term durability test, we observed that the FE_{NH_3} for Fe-MoS_2 nanosheets was maintained above 18% in the six rounds of successive reaction at -0.3 V *vs* RHE (Figs. 2d and S18). After the long-term test, the Fe-MoS_2 nanosheets were peeled

off the carbon paper with further analyses via TEM and XPS. The morphology and composition of Fe-MoS_2 nanosheets were still preserved (Figs. S19 and S20).

To explore the effect of the active site on N_2 electroreduction, we calculated the electrochemical surface area (ECSA) by measuring the double layer capacitance (C_{dl}).[41,42] The C_{dl} of Fe-MoS_2 nanosheets was 3.14 mF cm^{-2}, which was almost equal to that (3.17 mF cm^{-2}) of MoS_2 nanosheets (Figs. 3a and S21). Apparently, the difference in the activity between the two catalysts was independent of the ECSA. We also conducted the electrochemical impedance spectroscopy (EIS) measurements to explore the role of atomically dispersed Fe in Fe-MoS_2 nanosheets. It turned out that the charge transfer resistance (R_{ct}) of Fe-MoS_2 nanosheets was slightly smaller than that of MoS_2 nanosheets, indicating the faster electron transfer rate over Fe-MoS_2 nanosheets towards N_2 electroreduction (Fig. 3b). In addition, we also collected the LSV curves for Fe-MoS_2 and MoS_2 nanosheets in Ar-saturated electrolyte to explore their activity towards the competing HER (Fig. 3c). Based on the intercept of the linear region in Tafel plots, the exchange current density (j_0) for HER over Fe-MoS_2 nanosheets was calculated to be 109.6 μA cm^{-2}, which was visibly lower than that (138.0 μA cm^{-2}) over MoS_2 nanosheets. As a consequence, the activity of the competing HER over Fe-MoS_2 nanosheets was significantly suppressed compared to MoS_2 nanosheets (Fig. 3d).

To gain insight into the enhanced performance of N_2 electroreduction for Fe-MoS_2 nanosheets and investigate the effect of atomically dispersed Fe in Fe-MoS_2 nanosheets, we have employed density functional theory (DFT) calculations. The constructed model was established according to the EXAFS fitting data discussed above (Figs. S7, S8 and Table S2), where an Fe atom was coordinated with one S atom and three O atoms. The top view and side view of Fe-MoS_2 and MoS_2 structures were shown in Figure S22. In the simulation, the adsorption energy of N_2 adsorption was first examined on the Mo-edge for Fe-MoS_2 and MoS_2, respectively (Figs. S23 and S24). Then we screened possible intermediates and optimal pathways for N_2 electroreduction over Fe-MoS_2 and MoS_2 (Figs. 4a, S25, and S26a). For Fe-MoS_2, the reaction Gibbs free energy change (ΔG) of the PDS for hybrid pathway (N_2*→NNH*) was calculated as 0.37 eV. In comparison, the ΔG of the PDS for distal pathway (NNH_2*→N*) and for alternating pathway (NNH*→NHNH*) was 0.52 eV and 0.72 eV, respectively (Fig. 4, a and b). Therefore, we considered that the hybrid pathway served as the favorable pathway rather than the other two pathways over Fe-MoS_2. In addition, the N_2 electroreduction on MoS_2 also followed the distal

pathway as the ΔG of the PDS for distal pathway ($NNH_2^*\rightarrow N^*$) was 0.50 eV, lower than that (0.70 eV) of the PDS for alternating pathway ($NNH^*\rightarrow NNH_2^*$) (Fig. S26). Furthermore, for N_2 electroreduction, the energy barrier of the PDS for Fe-MoS_2 was 0.37 eV, which was lower than that (0.50 eV) for MoS_2 (Figs. 4b and S26b), indicating that the addition of atomically dispersed Fe facilitated N_2 electroreduction. Notably, the competing HER was also considered as it greatly influenced the selectivity of catalysts towards N_2 electroreduction. The calculated energy barriers for the competing HER was 0.15 eV for Fe-MoS_2 and 0.03 eV for MoS_2, respectively (Figs. 4c and S27), implying that the introduction of atomically dispersed Fe into MoS_2 nanosheets suppressed the competing HER, which was consistent with our experimental results of the exchange current density. The thermodynamic limiting potentials between the target product and the by-product (donated as U_L(target product)-U_L(by-product), where $U_L = -\Delta G'/e$, the $\Delta G'$ is the value of the reaction Gibbs free energy change for the PDS) is an important way to understand the competing mechanism.[43,44] A more positive value of $U_L(NH_3)$-$U_L(H_2)$ means a higher selectivity for N_2 electroreduction relative to HER. As shown in Figure 4d, Fe-MoS_2 exhibited a much more positive value (-0.22 V) for $U_L(NH_3)$-$U_L(H_2)$ than MoS_2 (-0.47 V), suggesting a higher selectivity for the electroreduction of N_2 on Fe-MoS_2.

In summary, we rationally developed Fe-MoS_2 nanosheets by the introduction of atomically dispersed Fe into MoS_2 nanosheets, which was proved to be an efficient catalyst for N_2 electroreduction. At -0.3 V *vs* RHE, Fe-MoS_2 nanosheets exhibited an FE_{NH_3} of 18.8% and the yield rate of NH_3 as high as 8.63 μg_{NH_3} $mg_{cat.}^{-1}$ h^{-1}. The mechanism study revealed that the N_2 electroreduction was facilitated on Fe-MoS_2 as the energy barrier of the PDS for Fe-MoS_2 was 0.37 eV, lower than that (0.50 eV) for MoS_2. Furthermore, the energy barrier for HER over Fe-MoS_2 was 0.15 eV, which was higher than that (0.03 eV) of MoS_2. As such, the introduction of atomically dispersed Fe on MoS_2 nanosheets suppressed the competing HER, thus enhancing the catalytic selectivity towards N_2 electroreduction. This work would provide a guideline for the rational design of novel and highly efficient Mo-based catalysts towards N_2 electroreduction by promoting N_2 electroreduction and suppressing HER process.

References

[1] C. H. Desch, *Nature* **1922**, *110*, 670-672.

[2] N. D. Spencer, R. C. Schoonmaker, G. A. Somorjai, *Nature* **1981**, *294*, 643-644.

[3] V. Rosca, M. Duca, M. T. de Groot, M. T. M. Koper, *Chem. Rev.* **2009**, *109*, 2209-2244.

[4] S. Licht, B. Cui, B. Wang, F.-F. Li, J. Lau, S. Liu, *Science* **2014**, *345*, 637-640.

[5] N. Lazouski, M. Chung, K. Williams, M. L. Gala, K. Manthiram, *Nat. Catal.* **2020**, *3*, 463-469.

[6] B. deB. Darwent, National Bureau of Standards, No. 31, Washington, DC, **1970**.

[7] J. W. Erisman, M. A. Sutton, J. Galloway, Z. Klimont, W. Winiwarter, *Nat. Geosci.* **2008**, *1*, 636-639.

[8] H. Liu, *Chin. J. Catal.* **2014**, *35*, 1619-1640.

[9] C. J. M. van der Ham, M. T. M. Koper, D. G. H. Hetterscheld, *Chem. Soc. Rev.* **2014**, *43*, 5183-5191.

[10] W. Guo, K. Zhang, Z. Liang, R. Zou, Q. Xu, *Chem. Soc. Rev.* **2019**, *48*, 5658-5716.

[11] S. Z. Andersen, V. Čolić, S. Yang, J. A. Schwalbe, A. C. Nielander, J. M. McEnancy, K. Enemark-Rasmussen, J. G. Baker, A. R. Singh, B. A. Rohr, M. J. Statt, S. J. Blair, S. Mezzavilla, J. Kibsgaard, P. C. K. Vesborg, M. Cargnello, S. F. Bent, T. F. Jaramillo, I. E. L. Stephens, J. K. Nørskov, I. Chorkendoff, *Nature* **2019**, *570*, 504-508.

[12] Y.-C. Hao, Y. Guo, L.-W. Chen, M. Shu, X.-Y. Wang, T.-A. Bu, W.-Y. Gao, N. Zhang, X. Su, X. Feng, J.-W. Zhou, B. Wang, C.-W. Hu, A.-X. Yin, R. Si, Y.-W. Zhang, C.-H. Yan, *Nat. Catal.* **2019**, *2*, 448-456.

[13] N. Cao, Z. Chen, K. Zang, J. Xu, J. Zhong, J. Luo, X. Xu, G. Zheng, *Nat. Commun.* **2019**, *10*, 2877.

[14] Z. Geng, Y. Liu, X. Kong, P. Li, K. Li, Z, Liu, J, Du, M. Shu, R. Si, J. Zeng, *Adv. Mater.* **2018**, *30*, 1803498.

[15] Y. Wang, M.-M. Shi, D. Bao, F.-L. Meng, Q. Zhang, Q. Zhou, Y.-T. Zhou, K.-H. Liu, , Y. Zhang, J.-Z. Wang, Z.-W. Chen, D.-P. Liu, Z. Jiang, M. Luo, L. Gu, Q.-H. Zhang, X.-Z. Cao, Y. Yao, M.-H. Shao, Y. Zhang, X.-B. Zhang, J. G. Chen, J.-M. Yan, Q. Jiang, *Angew. Chem. Int. Ed.* **2019**, *58*, 9464-9469.

[16] Y. Liu, Q. Li, X. Guo, X. Kong, J. Ke, M. Chi, Q. Li, Z. Geng, J. Zeng, *Adv. Mater.* **2020**, *32*, 1907690.

[17] J. Zhao, Z. Chen, *J. Am. Chem. Soc.* **2017**, *139*, 12480-12487.

[18] J. Zhao, J. Zhao, Q. Cai, *Phys. Chem. Chem. Phys.* **2018**, *20*, 9248-9255.

[19] R. Guo, M. Hu, W. Zhang, J. He, *Molecules* **2019**, *24*, 1777.

[20] Y.-Q. Le, J. Gu, W. Q. Tian, *Chem. Commun.* **2014**, *50*, 13319-13322.

[21] L. Han, X. Liu, J. Chen, R. Lin, H. Liu, F. Lv, S. Bak, Z. Liang, S. Zhao, E. Stavitski, J. Luo, R. R. Adzic, H. L. Xin, *Angew. Chem. Int. Ed.* **2019**, *58*, 2321-2325.

[22] L. Hui, Y. Xue, H. Yu, Y. Liu, Y. Fang, C. Xing, B. Huang, Y. Li, *J. Am. Chem. Soc.* **2019**, *141*, 10677-10683.

[23] L. Zhang, X. Ji, X. Ren, Y. Ma, X. Shi, Z. Tian, A. M. Asiri, L. Chen, B. Tang, X. Sun, *Adv. Mater.* **2018**, *30*, 1800191.

[24] X. Ren, J. Zhao, Q. Wei, Y. Ma, H. Guo, Q. Liu, Y. Wang, G. Cui, A. M. Asiri, B. Li, B. Tang, X. Sun, *ACS Cent. Sci.* **2019**, *5*, 116-121.

[25] H. Cheng, L.-X. Ding, G.-F. Chen, L. Zhang, J. Xue, H. Wang, *Adv. Mater.* **2018**, *46*, 1803694.

[26] C. E. Mckenna, J. B. Jones, H. Eran, C. W. Huang, *Nature* **1979**, *280*, 611-612.

[27] F. Jiao, B. Xu, *Adv. Mater.* **2018**, *31*, 1805173.

[28] T. F. Jaramillo, K. P. Jorgensen, J. Bonde, J. H. Nielsen, S. Horch, I. Chorkenodorff, *Science* **2007**, *317*, 100-102.

[29] W. Wu, C. Niu, C. Wei, Y. Jia, C. Li, Q. Xu, *Angew. Chem. Int. Ed.* **2019**, *58*, 2029-2033.

[30] J. Xie, H. Zhang, S. Li, R. Wang, X. Xun, M. Zhou, J. Zhou, X. W. Lou, Y. Xie, *Adv. Mater.* **2013**, *25*, 5807-5813.

[31] Y. Shi, Y. Zhou, D.-R. Yang, W.-X. Xu, C. Wang, F.-B. Wang, J.-J. Xu, X.-H. Xia, H.-Y. Chen, *J. Am. Chem. Soc.* **2017**, *139*, 15479-15485.

[32] Y. Lan, E. C. Butler, *Environ. Sci. Technol.* **2016**, *50*, 5489-5497.

[33] Z. Yang, M. Kang, B. Ma, J. Xie, F. Chen, L. Charlet, C. Liu, *Environ. Sci. Technol.* **2014**, *48*, 10716-10724.

[34] I. Uhlig, R. Szargan, H. W. Nesbitt, K. Laajalehto, *Appl. Surf. Sci.* **2001**, *179*, 222-229.

[35] T. Yamashita, P. Hayes, *Appl. Surf. Sci.* **2008**, *254*, 2441-2449.

[36] E. Murad, *Pure Appl. Chem.* **2015**; *87*, 301-306

[37] M.-E. Pandelia, N. D. Lanz, S. J. Booker, C. Krebs, *Biochimica et Biophysica Acta* **2015**, *1853*, 1395-1405

[38] E. Kuchma, S. Kubrin, A. Soldatov, *Biomedicines* **2018**, *6*, 78

[39] C. A. Apblett, D. M. Stewart, R. T. Fryer, J. C. Sell, P. Harry D. III, T. M. Anderson, R. W. Meulenberg, *Electrochim. Acta* **2015**, *185*, 156-161.

[40] D. Bao, Q. Zhang, F.-L. Meng, H.-X. Zhong, M.-M. Shi, Y. Zhang, J.-M. Yan, Q. Jiang, X.-B. Zhang, *Adv. Mater.* **2017**, *29*, 1604799.

[41] J. Li, Y. Wang, T. Zhou, H. Zhang, X. Sun, J. Tang, L. Zhang, A. M. Al-Enizi, Z. Yang, G. Zheng, *J. Am. Chem. Soc.* **2015**, *137*, 14305-14312.

[42] F. Song, X. Hu, *Nat. Commun.* **2014**, *5*, 4477.

[43] D. Kim, C. Xie, N. Becknell, Y. Yu, M. Karamad, K. Chan, E. J. Crumlin, J. K. Norskov, P. Yang, *J. Am. Chem. Soc.* **2017**, *139*, 8329-8336.

[44] C. Shi, H. A. Hansen, A. C. Lausche, J. K. Norskov, *Phys. Chem. Chem. Phys.* **2014**, *16*, 4720-4727.

10.1002/anie.202009217

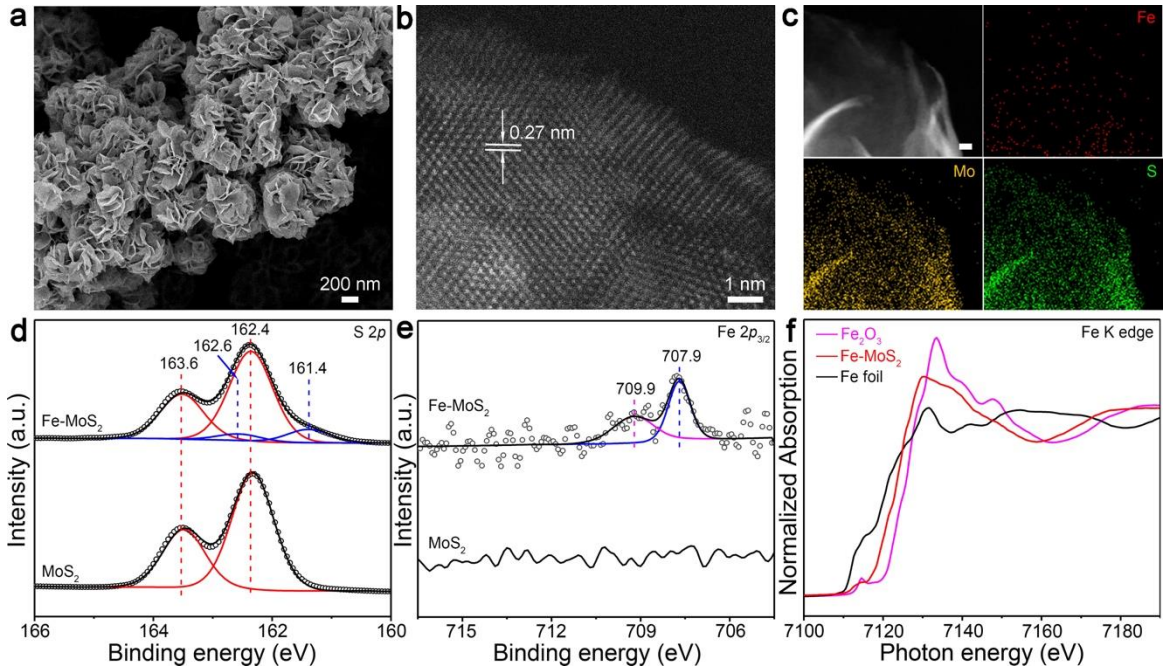

Figure 1. (a) SEM image and (b) HAADF-STEM image of Fe-MoS_2 nanosheets. (c) HAADF-STEM and STEM-EDX elemental mapping images of Fe-MoS_2 nanosheets. The scale bar in the HAADF-STEM image in (c) represents 10 nm. (d) S 2*p* and (e) Fe $2p_{3/2}$ XPS spectra of Fe-MoS_2 and MoS_2 nanosheets. (f) Normalized XANES spectra at the Fe K edge of Fe-MoS_2 nanosheets, Fe_2O_3, and Fe foil.

10.1002/anie.202009217

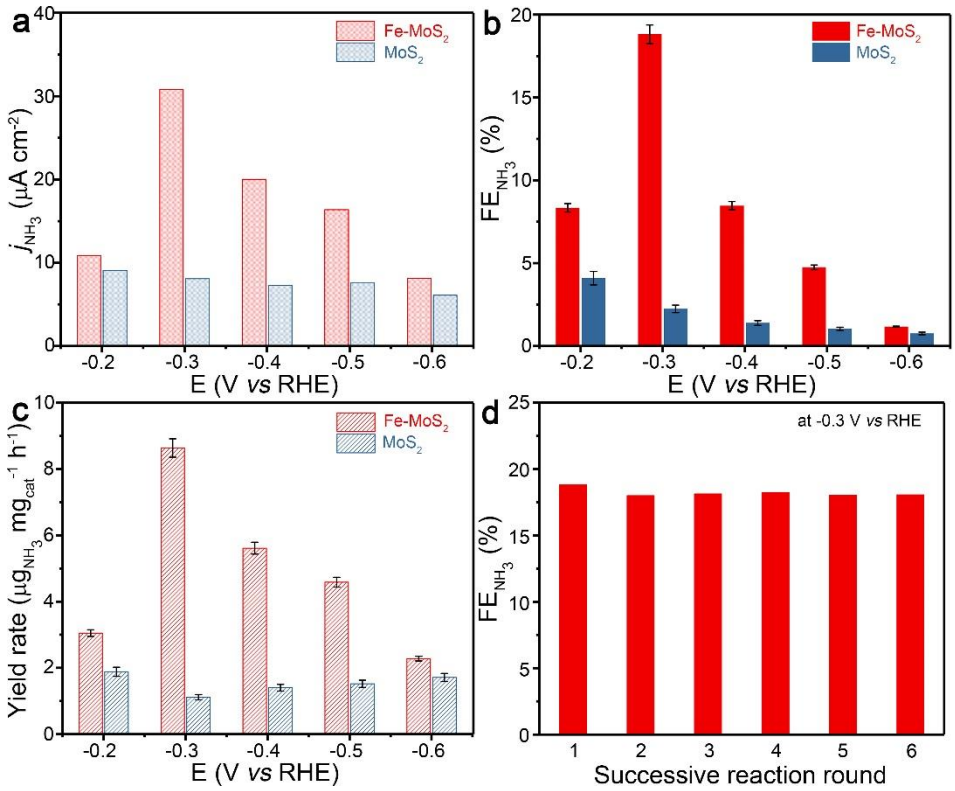

Figure 2. (a) j_{NH_3}, (b) FE, and (c) Yield rate of NH_3 for Fe-MoS_2 and MoS_2 nanosheets towards N_2 electroreduction at different applied potentials. (d) FE of NH_3 for Fe-MoS_2 nanosheets at the potential of -0.3 V *vs* RHE with six rounds of successive reactions.

10.1002/anie.202009217

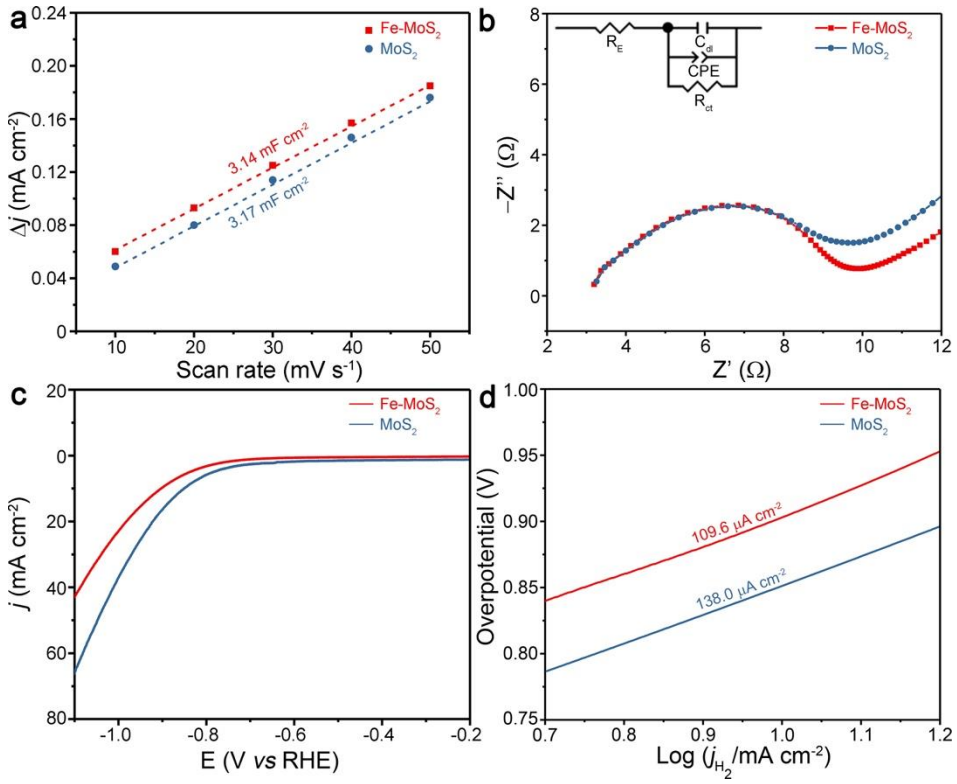

Figure 3. (a) Charging current density differences plotted against scan rates, (b) Nyquist plots for Fe-MoS_2 and MoS_2 nanosheets, (c) LSV curves for Fe-MoS_2 and MoS_2 nanosheets in Ar-saturated electrolyte. The sweeping rate is 10 mV s^{-1} for both curves. (d) Tafel plots of Fe-MoS_2 and MoS_2 nanosheets in Ar-saturated electrolyte. The exchange current densities (j_0) for HER were derived from the intercept of the linear region in Tafel plots.

10.1002/anie.202009217

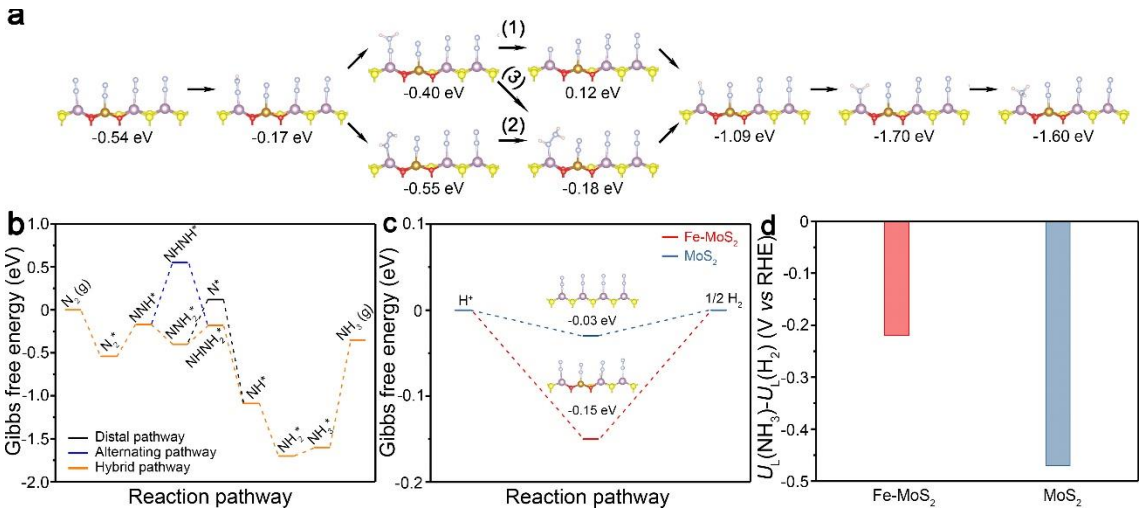

Figure 4. (a) Schematic illustrations showing the (1) distal, (2) alternating, and (3) hybrid pathways for N_2 electroreduction over the Mo-Mo bridge of Fe-MoS_2 (Mo-edge) structure. The numbers in (a) indicate the calculated Gibbs free energy of each corresponding configuration. (b) Gibbs free energy for N_2 electroreduction following the distal, alternating, and hybrid pathway in (a). (c) Gibbs free energy for HER over Fe-MoS_2 and MoS_2. (d) Differences in thermodynamic limiting potentials for N_2 electroreduction and HER over Fe-MoS_2 and MoS_2. The spheres with various colors represent Fe (brown), Mo (violet), S (yellow), N (light blue), O (red), and H (light pink), respectively. * represents an adsorption site.